Hindawi
Journal of Sensors
Volume 2023, Article ID 9810493, 1 page
https://doi.org/10.1155/2023/9810493

Retraction

Retracted: Research Progress on the Molecular Mechanism of EGCG3″Me in the Treatment of Diabetes Based on Visual Sensor Images

Journal of Sensors

Received 22 August 2023; Accepted 22 August 2023; Published 23 August 2023

This article has been retracted by Hindawi following an investigation undertaken by the publisher [1]. This investigation has uncovered evidence of one or more of the following indicators of systematic manipulation of the publication process:

(1) Discrepancies in scope
(2) Discrepancies in the description of the research reported
(3) Discrepancies between the availability of data and the research described
(4) Inappropriate citations
(5) Incoherent, meaningless and/or irrelevant content included in the article
(6) Peer-review manipulation

The presence of these indicators undermines our confidence in the integrity of the article's content and we cannot, therefore, vouch for its reliability. Please note that this notice is intended solely to alert readers that the content of this article is unreliable. We have not investigated whether authors were aware of or involved in the systematic manipulation of the publication process.

Wiley and Hindawi regrets that the usual quality checks did not identify these issues before publication and have since put additional measures in place to safeguard research integrity.

We wish to credit our own Research Integrity and Research Publishing teams and anonymous and named external researchers and research integrity experts for contributing to this investigation.

The corresponding author, as the representative of all authors, has been given the opportunity to register their agreement or disagreement to this retraction. We have kept a record of any response received.

References

[1] G. Li, X. Du, and Z. Li, "Research Progress on the Molecular Mechanism of EGCG3″Me in the Treatment of Diabetes Based on Visual Sensor Images," *Journal of Sensors*, vol. 2021, Article ID 2541214, 11 pages, 2021.

Hindawi
Journal of Sensors
Volume 2021, Article ID 2541214, 11 pages
https://doi.org/10.1155/2021/2541214

Research Article

Research Progress on the Molecular Mechanism of EGCG3″Me in the Treatment of Diabetes Based on Visual Sensor Images

Guiwen Li,[1] Xianfeng Du ,[1] and Zhengkang Li[2]

[1]*College of Tea and Food Science and Technology, Agriculture University of Anhui, Hefei, 230036 Anhui, China*
[2]*College of Electronics and Information, South China University of Technology, Guangzhou, 510641 Guangdong, China*

Correspondence should be addressed to Xianfeng Du; gaojun771002@ahau.edu.cn

Received 3 September 2021; Revised 25 October 2021; Accepted 28 October 2021; Published 10 December 2021

Academic Editor: Haibin Lv

Diabetes is a chronic metabolic disease with abnormal blood glucose and lipid metabolism caused by insufficient insulin secretion, which seriously affects human health. For solving the problem of treating diabetes, it is particularly important to observe the research progress of the molecular mechanism of EGCG3″Me in the treatment of diabetes based on visual sensor images. This research has not been verified in practice, but many scientists are already studying it. This article is aimed at studying the molecular mechanism of using EGCG3″Me to treat diabetes based on visual sensor images. This article introduces the concept and application of visual image sensor in detail, using a superpixel segmentation method to realize image observation. The EGCG3″Me was extracted and used in diabetes treatment experiments. The experimental results showed that the blood glucose of the mice in the experimental group had returned to normal 60 minutes after the administration of glucose in the blank control group, and the blood glucose of the mice in the control group had basically returned to normal after 120 minutes. Compared with the model group, the number of acinar paging and the number of cells in the pancreatic islets increased in the mice after EGCG3″Me treatment, indicating that EGCG3″Me has the effect of protecting and repairing pancreatic islet cells.

1. Introduction

1.1. Background. Diabetes mellitus (DM) is a disease of systemic metabolic disorder. It is mainly manifested by hyperglycemia. Metabolic disorder is a state of the body, which is a state where the body's digestion, absorption, and excretion of substances appear pathological and unbalanced. It can be manifested as a disorder of one substance or multiple substances. It is divided into type 1 and type 2 according to the cause, pathogenesis, and clinical manifestations. 90%-95% of them are type 2 diabetes (T2DM). Although various drugs for the treatment of DM are constantly updated, it is a pity that the morbidity and mortality of DM in most countries, including our country, have not significantly reduced. DM has seriously endangered human life and health. Therefore, the effective prevention and treatment of DM has become a hot spot of global concern, and it is also a major issue that needs to be solved urgently in our country. Research and development of new prevention and treatment methods and ideas is still the primary task of overcoming DM.

1.2. Significance. Diabetes is a chronic metabolic disease caused by insufficient insulin secretion due to abnormal blood sugar and blood lipid metabolism, which seriously affects human health. The information is extracted from the human target cells through the visual sensor, and then the pathological conditions of the cells are analyzed by analyzing the extracted image features, and then a suitable treatment plan is found. Therefore, to clarify its pathogenesis and find effective therapeutic targets has important theoretical significance and practical value. In hyperglycemia, excessive secretion of ROS in cells causes a series of damaging effects. Nrf2 is an important protective factor for diabetes. Improving the antioxidant pathway of Nrf2 has a certain preventive effect on the prevention and treatment of diabetes. EGCG3″Me is a potent Nrf2 agonist, which can activate the Nrf2 antioxidant signal pathway and initiate the expression of downstream antioxidant genes heme oxygenase 1 and reduced coenzyme/quinone oxidoreductase 1. Nrf2 is an important protective factor for diabetic complications; increasing the expression of Nrf2 in the body can effectively

alleviate diabetic complications; as a Nrf2 agonist, EGCG3″Me has obvious effects on oxidative stress, inflammation, and apoptosis caused by diabetes. It is of great significance to study the role and related mechanisms of EGCG3″Me in the treatment of DNHW. How to control the operation mechanism of Nrf2 during the experiment is a question worth pondering. In the experiment, this article describes how to control the operation of Nrf2.

1.3. Related Work. At present, the incidence of diabetes is high and there are many complications. Qin and Wang pointed out that at present, the target vehicle detection method based on monocular vision sensor takes the whole vehicle as the target [1]. Abbasi et al. pointed out that this article introduced vision-based aerial robot formation flight control, with special attention to failures in visual communication [2]. Masson et al. pointed out that the LIRIS demonstrator is a vision-based navigation sensor experiment, implemented on the ATV-5 George Lemaitre, and activated during the approach phase with the International Space Station (ISS) [3]. Sakuma et al. pointed out that skeletal muscle provides the basic foundation for human function, making movement and breathing possible. Muscle loss is the result of several chronic diseases (cachexia) and normal aging (sarcopenia) [4]. Bosona et al. pointed out that this article introduced the results of a study on the dynamic response of camels' heart rate (HR) under working conditions. The main goal is to develop a simulation model that can describe the dynamic characteristics of the camel's heart rate on physical activity, that is, pulling the loaded trolley and sled [5]. Choi pointed out that the Bionic Micro Suction Cup (mSC) is specifically designed for patient-friendly smart medical skin dry adhesives. The strong van der Waals force and induced negative pressure generated by the super soft mSC promote tight skin coupling without discomfort or irritation and improve the sensitivity of embedded stretchable electronic devices for continuous vital sign monitoring [6]. Although these studies did not combine vision sensors with the treatment of diabetes, this article can be modified in conjunction with their ideas, and the unique functions of the article can be used for processing, and finally, the method studied in this article can be derived.

1.4. Main Content. EGCG3″Me is the main component of Tieguanyin tea polyphenols. It is a catechin-like monomer isolated from tea. It has antibacterial, antioxidant, antiarteriosclerosis, antivascular proliferation, and anti-inflammatory effects. However, the research on its therapeutic effect on diabetes is still shallow; especially, its protective effect on pancreatic function has not been fully investigated. This study will start from glucose and lipid metabolism and study the effect of EGCG3″Me on improving blood glucose and lipid metabolism and pancreatic islet secretion in diabetic mice. This article first introduces the concept and application technology of the visual image sensor and then introduces the extraction of EGCG3″Me in detail. Experiments were carried out by establishing a diabetic mouse model. In this study, through glucose-stimulated insulin release experiments and pancreatic HE staining, it was found that the pancreatic islet cells in the diabetic group were significantly damaged, the number of acinar paging increased, and the number of cells in the pancreatic islets decreased.

2. Molecular Mechanism Research Methods

2.1. Visual Function Repair. The formation of vision requires a complete visual system [7, 8]. The visual system is the most complex organ of human sense organs in function and structure. The earliest research on visual prostheses was Brindley and his contemporaries Dobell. By using a part of the implanted electrodes to stimulate the cerebral cortex, people produce phantom vision. The subretinal prosthesis is replaced by a miniature photodiode array [9, 10]. The photoreceptor cells have lost their function, and the image information is processed through the axon network of the inner retina of the eyeball. There is no need to add photoreceptors and processing systems, and the structure is simple. Because the development of visual cortex prostheses and optic nerve prostheses is difficult, they are far inferior to retinal prostheses. In the current research, the external image sensor is generally used; that is, the image acquisition and processing unit circuits are located outside the eyeball, and the processed signal is transmitted to the microelectrode array of the microstimulator implanted in the eyeball through wireless communication. Wearing an external camera and image processing unit, the camera cannot expand the field of view with the rotation of the eyeball, which does not conform to normal eye habits, and is unsightly to wear, which is not conducive to protecting the privacy of users with visual defects. Another method is to use a built-in image sensor [11]; that is, a camera implanted in the eyeball is used to collect image information from the outside world. Due to the large pixel unit of the existing image sensor on the market, the collected image information needs to be digitally signaled. The processor DSP can transmit to the microstimulator and microelectrode array after processing, and the subsequent processing circuit is more complicated, which leads to the large overall volume and power consumption of the image acquisition and processing system, which is not suitable for intraocular use, which requires special design. Image sensor and image signal processing circuit are used to reduce power consumption and volume. After processing by the processor DSP, it can be transmitted to the microstimulator and the microelectrode array, which will affect the image receipt process in the experiment, making the picture incomplete. The energy supply of the visual prosthesis can be achieved through wireless transmission. The superpixel segmentation method can extract insulin molecules in the human body and then analyze the extracted images to determine whether the pancreatic islet cells are diseased.

2.2. Visual Image Sensor

2.2.1. Image Sensor. And image sensor products have become the object of current and future industry attention, attracting investment from many manufacturers. The real image sensor uses the photoelectric effect of the photodiode to convert the input image signal into an electrical signal and

integrates the pixel array, timing control, signal processing, etc. on the same semiconductor substrate to realize the conversion of image light signals to electrical signals. Vacuum image sensors, such as electron beam camera tubes, are difficult to apply on a large scale due to their high cost, being bulky, and being inconvenient manufacturing equipment due to the easy distortion of images. In contrast, solid-state image sensors have low image distortion [12], small size, high integration, low power consumption, and strong antielectromagnetic interference capabilities. Solid-state image sensors are also known as imaging equipment or camera originals, which can detect visible light, ultraviolet, X-ray, and near-infrared light. It is a basic equipment for obtaining visual information in modern times. Because it can realize the reading and conversion of information and the expansion of visual functions and can provide visual image information that is intuitive, true, multilevel, and multicontent, image sensors are being used more and more widely in modern science and technology. It is mainly used in the image evaluation system of image sensor product research and development, manufacturing inspection, and function demonstration. This article combines it with medical images to find out pathological conditions by analyzing the morphology of target cells. The sensor data acquisition process is shown in Figure 1.

2.2.2. Wireless Image Sensor Node. With the continuous development of information technology, wireless image sensor nodes have gradually become one of the research hotspots.

The design of the wireless image sensor node can depend on the specific application. In the case of ensuring energy supply, if the specific application field has higher requirements for data processing capabilities, you can use high-performance processors [13] and other related hardware. For example, SensEye has made some attempts in this regard. SensEye uses a higher-performance Mini-ITX. In order to accelerate the application development process, the image acquisition part of the wireless image sensor node can use a ready-made camera or video camera. Similarly, not all communication modules of the sensor nodes described above use Zigbee series chips. For example, some researchers use nRF24L01 chips. This also reflects the flexibility of the current wireless sensor node design [14]. The amount of data to be transmitted is very small, which will provide a larger space for the choice of node communication methods. We believe that the design of wireless image sensor nodes and their communication methods can be determined by specific application requirements. The high-performance processor is one of the main equipment of electronic computers and the core accessory in the computer. Its function is mainly to interpret computer instructions and process data in computer software. The CPU is the core component of the computer that is responsible for reading instructions and decoding and executing instructions. The application of the image sensor is shown in Figure 2. Among them, VR and AR have higher requirements for visual sensors, because they require powerful real-time performance and high throughput.

2.3. Machine Vision Applied to Vision Sensors. The so-called machine vision can be simply thought of as making the machine have a certain "visual ability" in some aspects in order to complete some tasks. The machine [15, 16] can be used to imitate human vision, and the machine can also imitate the vision of other creatures to help humans complete some tasks. These tasks may be difficult for human eyes to complete. At present, the research of vision measurement and vision control based on machine vision has also become a research hotspot. It can be considered that the processing process of vision measurement is to capture the relevant image of the measured object through the image sensor and then process the relevant image, so as to further obtain the relevant information of the measured object that the user needs. On the basis of visual measurement research, some scholars have studied visual control to obtain necessary information through visual measurement to control the machine. Obviously, visual measurement will provide important help for the control of robots or other equipment. The research content of machine vision involves embedded technology, image acquisition, image processing, pattern recognition, image sensor technology, and many other fields. Because it involves a wide range of fields, it is used in many embedded systems. The system obtains image information through image sensors and processes image information, so as to achieve the purpose of measurement and detection. Machine vision has the advantages of high accuracy [17] and long continuous working time. People can not only make machines imitate human vision but also make machines imitate the vision of some other creatures. For example, visual bionic technology such as electronic frog eyes has been studied by many scholars. In places where the human eye is incompetent, machine vision can be used to replace human vision and help humans work to avoid risks. In real life and work, people use their eyes for a long time, it will cause visual fatigue, and the accuracy will be reduced, but machine vision can avoid this problem. This will greatly improve production efficiency. In summary, this article believes that with the development of machine vision, the study of machine vision for wireless image sensor nodes will have important research significance.

Machine vision has been applied in some fields, showing its important research value. Machine vision systems have broad application prospects in many fields. According to relevant information, if the driver receives an alarm 1 second before the collision, the accident can be reduced by about 90%. Therefore, it is very meaningful to study the relevant alarm system. The open source algorithm library and program is a free shared code library written by many programmers. Its purpose is to make it easy for each programmer to find the algorithms and programs he needs. Many software and algorithm libraries related to machine vision have appeared; there are also a large number of [18, 19] open source algorithm libraries and programs written by algorithm enthusiasts that have been released for free in many ways. All these great methods have promoted the research of machine vision related algorithms. The related research of machine vision also involves many fields. For example, machine vision can be used for fingerprint recognition, face

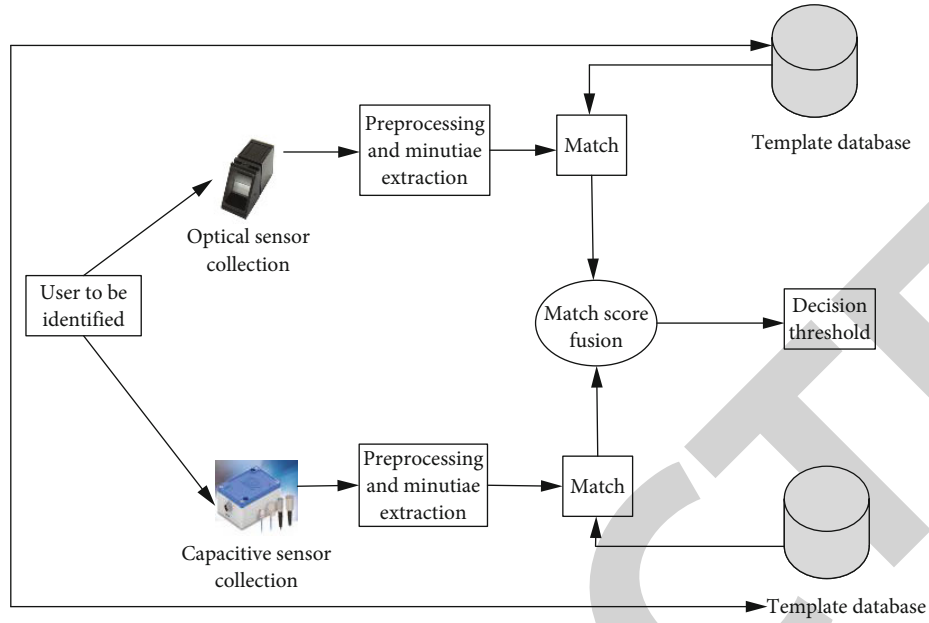

Figure 1: Sensor data collection.

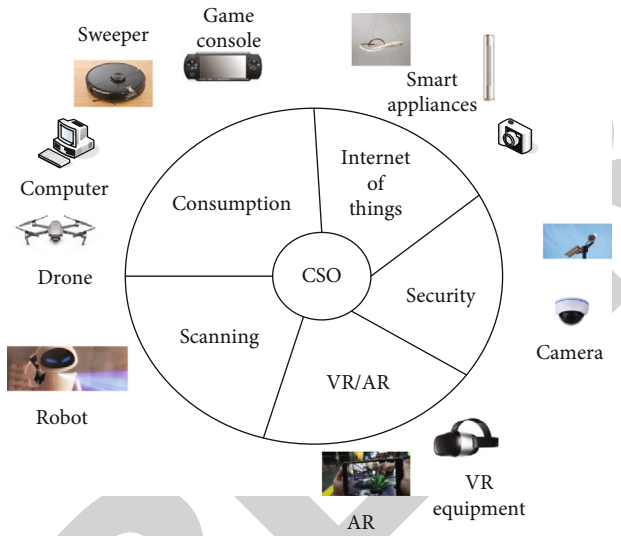

Figure 2: Image sensor application.

recognition, iris recognition, printing inspection, BGA package inspection and punching board inspection, and so on. In addition to letting the machine imitate human vision [20], it can also let the machine simulate the "vision" of some other creatures. For example, technologies like electronic frog eyes have an important application value.

2.4. Digital Pixel Image Sensor and Image Segmentation Algorithm. The CMOS digital pixel image sensor integrates an A/D converter [21] on the pixel unit to output digital signals. The principle block diagram is shown as in Figure 3. Pixel-level ADC can use one pixel to integrate one ADC or use several adjacent pixels (pixel blocks) to integrate one ADC, so that the pixels in the pixel block share this ADC. The ADC in each pixel is converted at the same time and read out in parallel, so the speed of the ADC can be very low. Compared with analog image sensors, due to the reduced performance requirements of analog circuits, the chip can be scaled down better with the CMOS process; the readout fixed pattern noise (FPN) and column readout noise are reduced. An ADC and memory are used in each pixel to perform parallel A/D conversion, and the readout signal is a digital signal, which can realize high-speed reading, which is very suitable for traditional high-speed imaging applications. However, DPS needs to use more transistors in each pixel, the fill factor is smaller, and the pixel size is larger than that of the traditional analog image sensor. In Figure 3, PD is a value, and ADC refers to an analog/digital converter or an analog/digital converter. It refers to the screen that converts analog signals of continuous variables into discrete digital signals and final output.

2.4.1. Parameter Active Contour Model. In a parametric active contour model, snake is a curve, $X(s) = [x(s), y]$ closed parametric curve $C(s) = (x), y(s) = (x), y(s) = (x)$, $y(s)$ is the given gray-scale image, and the parameter $s[0, 1]$; the total energy expression is as follows:

$$E(X(s)) = \int_0^1 [E_{\text{int}}(X(s)) + E_{\text{ext}}(X(s))ds]. \quad (1)$$

The energy function E above is the functional of the $X(s)$ vector function, and E_{int} represents the internal energy functional, which is composed of its own geometric characteristics, and its role is to maintain the smooth continuity of the evolution curve. Its expression is as follows:

$$E_{\text{int}}(X(s)) = \frac{1}{2}\left[\alpha(s)\left|X'\right|^2 + \beta(s)\left|X''(s)\right|^2\right]. \quad (2)$$

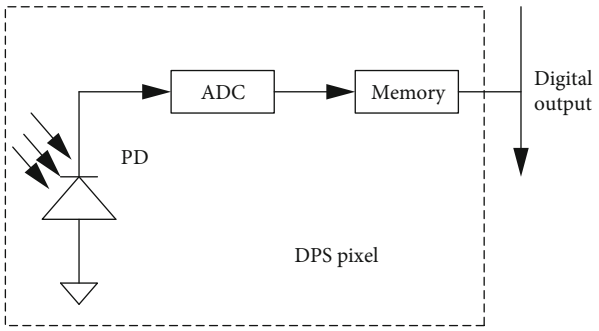

Figure 3: Simple DPS pixel unit structure.

$E_{\text{ext}}(X(s))$ represents the external energy functional. The external energy functional is as follows:

$$E_{\text{ext}}(X(s)) = E_{\text{img}}(X(s)) + E_{\text{con}}(X(s)). \tag{3}$$

Among them, $E_{\text{img}}(X(s))$ is the image energy, and $E_{\text{con}}(X(s))$ is the external constraint energy. The image energy functional $E_{\text{img}}(X(S))$ is as follows:

$$E_{\text{img}}(X(s)) = |\nabla I(x, y)|^2. \tag{4}$$

The effect of segmentation is very good, and this method is automatic segmentation, which is a convenient and effective method of segmentation.

2.4.2. Geometric Active Contour Model. The level set method is a numerical technique used for interface tracking and shape modeling. The advantage of the level set method is that the evolving curve and surface can be numerically calculated on the Cartesian grid without parameterizing the curve and surface. Another advantage of the level set method is that it can easily track changes in the topological structure of the object. For example, when the shape of the object is divided into two: a hole generated or the reverse operation. All of these make the level set method a time-varying object construction. The powerful tool of the mold, such as an inflating airbag, drops oil into the water.

The geometric active contour model is mainly based on the level set method. The basic theory of the level set method is as follows: the curve $C(t)$ is obtained from the zero level set of the level set function φ ($\phi(C(t), t)$ is the level set function at time t).

$$C(t) = \{\varphi(C(t), t) = 0\}. \tag{5}$$

From $\phi(C(t), t) = 0$, to fully differentiate t, we can get

$$\frac{\partial \phi}{\partial t} + \nabla \phi \cdot \frac{\partial C}{\partial t} = 0. \tag{6}$$

In the above formula, $\nabla\phi$ represents the gradient of φ. In addition, from mathematical knowledge, it can be known that $\nabla\phi$ is perpendicular to the tangent line of curve C; that is to say, $\nabla\phi$ is the same as the normal direction of the curve. Then, the unit normal vector $\vec{N}$ of the curve can be obtained according to the following formula:

$$\vec{N} = -\frac{\nabla \varphi}{|\nabla \varphi|}. \tag{7}$$

The curve evolution equation of the level set is as follows:

$$\begin{cases} \dfrac{\partial \varphi}{\partial t} + F|\nabla \varphi| = 0, \\ \varphi(0, x, y) = \varphi_0(x, y). \end{cases} \tag{8}$$

The corresponding distance function is as follows:

$$\varphi = \begin{cases} -d((x, y), C), & (x, y) \text{ inside the curve}, \\ 0, & (x, y) \text{ on the curve}, \\ d((x, y), C), & (x, y) \text{ outside the curve}. \end{cases} \tag{9}$$

d means finding the Euclidean distance from the point to the curve. The edge indicator function g is as follows:

$$g = \frac{1}{1 + |\nabla(G_\sigma * I)|^2}. \tag{10}$$

The image segmentation formula of the level set method is as follows:

$$\frac{\partial \varphi}{\partial t} = g|\nabla \varphi| \left(\text{div} \left(\frac{\nabla \varphi}{|\nabla \varphi|} \right) + v \right). \tag{11}$$

2.4.3. Local Contrast. Local contrast is a method of comparing only the regions with the highest similarity in a given sequence. It is suitable for sequences that have high similarity in some parts and large differences in other parts.

Many saliency calculation methods use local contrast, which mainly obtains the saliency value of a region by comparing the pixel characteristics of a region with its neighboring regions. According to the regional consistency theory, if the features of the regions are similar and the spaces are similar, then, these regions should have similar significant values. For a super pixel, its local saliency value relative to all other super pixels can be defined as follows:

$$B(i) = \sum_{j=1}^{N} D_F(i, j) \times D_s(i, j) \times f(j). \tag{12}$$

Among them, the first term $D_F(i, j)$ of Equation (12) represents the dissimilarity between two superpixel features, which is simply defined as the difference between the two superpixel features:

$$\sum_{j=1}^{N} D_F(i, j) = |F(i) - F(j)|. \tag{13}$$

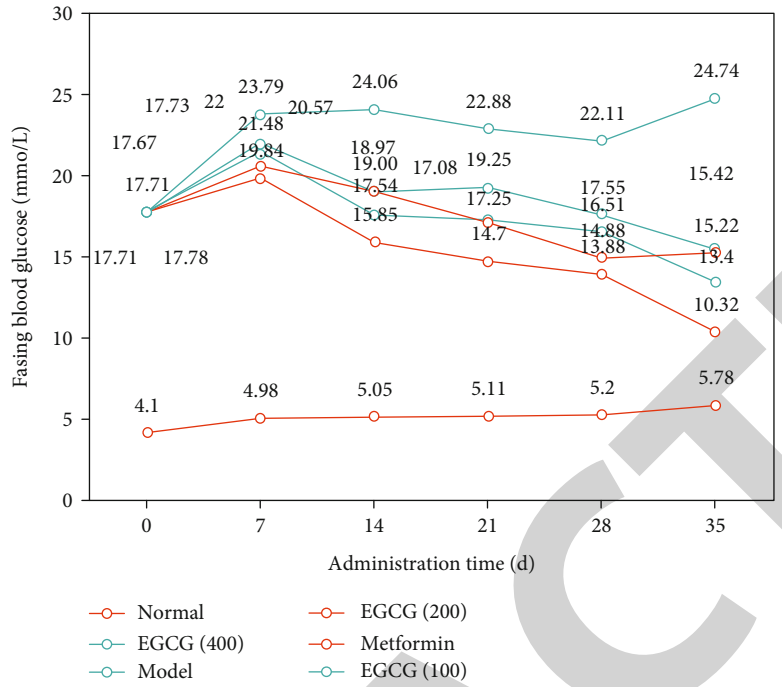

Figure 4: The effect of EGCG3″Me on fasting blood glucose ($\bar{x} \pm s$, $n = 11$).

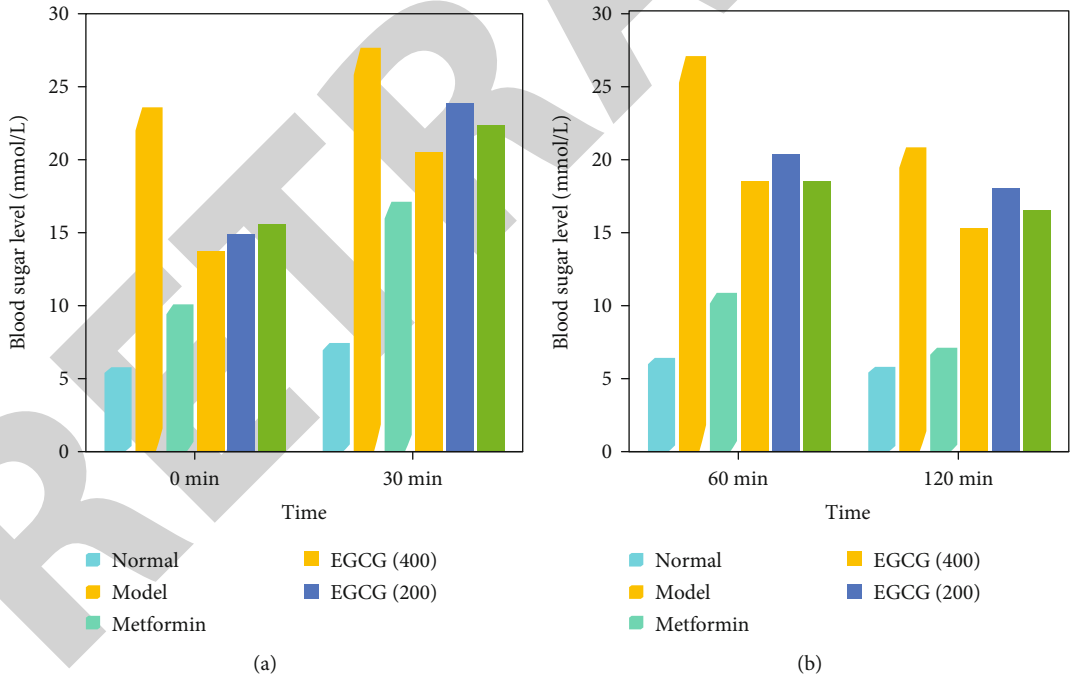

Figure 5: Comparison of the effect of EGCG3″Me on glucose tolerance in diabetic mice ($\bar{x} \pm s$, $n = 11$). (a) Within 30 minutes. (b) Within 60-120 minutes.

The second term $D_s(i, j)$ of Equation (12) represents the spatial relationship between two superpixels.

$$D_s(i,j) = \exp\left[\frac{\left[\left(x_i - x_j\right)/M\right]^2 + \left[\left(y_i - y_j\right)/N\right]^2}{2\sigma_o^2}\right]. \quad (14)$$

Among them, (x_i, y_i) is the centroid of the super pixel i, as the position of the super pixel, the size of the image I is MXN, and σ_o is the scale parameter, which controls the spatial weighting. The last term $f(j)$ in Equation (12) represents the relative size of superpixel j, and $S(\cdot)$ represents the size of the superpixel area. Then, the relative size of superpixel j is defined as follows:

Table 1: Effect of EGCG3″Me on glucose-stimulated insulin release in diabetic mice ($\bar{x} \pm s$, $n = 11$).

Group	Dose	G10	In0	In10	Insulin increase rate
Normal	—	9.25 ± 2.52	53.53 ± 10.26	192.62 ± 44.71	$2.80 \pm 1.31^{\#\#}$
Model	—	$64.41 \pm 10.82^{\#\#\#}$	$8.34 \pm 3.88^{\#\#\#}$	$20.87 \pm 12.48^{\#\#}$	$1.37 \pm 0.76^{\#\#}$
Metformin	400	$37.13 \pm 15.84^{***}$	$12.80 \pm 5.62^{*}$	33.26 ± 25.68	0.97 ± 0.35
EGCG3″Me high dose	400	$44.12 \pm 11.40^{***}$	$11.74 \pm 5.07^{*}$	$31.51 \pm 13.03^{*}$	$2.08 \pm 0.64^{*}$
EGCG3″Me medium dose	200	$49.56 \pm 9.81^{***}$	10.12 ± 4.47	$31.15 \pm 15.15^{*}$	$2.28 \pm 1.11^{*}$
EGCG3″Me low dose	100	$48.09 \pm 6.29^{***}$	$10.77 \pm 3.40^{*}$	$28.24 \pm 12.19^{*}$	2.50 ± 1.99

Compared with the blank group, $^{\#\#}P < 0.01$ and $^{\#\#\#}P < 0.001$; compared with the model group, $^{*}P < 0.05$, $^{**}P < 0.01$, and $^{***}P < 0.001$.

$$f(j) = \frac{S(j)}{S(I)}. \tag{15}$$

On the basis of analyzing the defects of traditional feature-level fusion algorithms, the feature fusion theory proposes to achieve fusion through the three steps of feature vector relationship projection, projection fusion, and dimensionality reduction under the subspace framework, to fundamentally solve the feature space involved in feature fusion incompatibility, dimensionality inconsistency, high-dimensional disasters, and other theoretical problems; it overcomes the problems caused by the correlation between the two-dimensional dimensionality reduction and confusion between feature vectors and the independence between multiple modes and achieves more than decision-level fusion, with excellent results.

As shown in Formula (12), the local contrast saliency of a superpixel is related to the dissimilarity, spatial distance, and relative size of the compared area; that is, the closer the distance, the more dissimilar and larger the superpixel area to the current superpixel and the greater the influence of the region. According to the feature fusion theory, the initial saliency map of the image is obtained by fusing Formulas (12) and (13).

$$S_{\text{in}}(i) = A(i) \times B(i). \tag{16}$$

Smooth connection involves the Euclidean distance that needs to be calculated in the geometric active contour model of the parameterized active contour model.

3. EGCG3″Me Treatment of Diabetes Experiment

3.1. Extraction of EGCG3″Me. Take 95% of 100 grams of Tieguanyin tea polyphenols, dissolve it in 2000 mL of water, and reversely extract with 1/2 to 1/4 volume of ethyl butyrate for 3 to 4 times, and discard the ethyl butyrate phase. The obtained water phase is evaporated and concentrated to 1/2 to 1/3 of the original volume to remove residual ethyl butyrate in the water. Then, an equal volume of propyl acetate phase is used to countercurrently extract 2 to 3 organic phases, and vacuum evaporation and concentration drying are performed. The dried crude extract was dissolved in 2000 mL of water with 20 mol/dm^3 aluminum sulfate solution, after a period of precipitation, filtered, washed with hot water at 60°C for 2~3 times, and then washed with 3°C~5°C hydrochloric acid (HCI) solution. The method of vacuum evaporation and recrystallization is adopted to realize the method of eluting the acid with water in the organic phase. Freeze dry, that is, pure white EGCG3″Me children's tea products. The prerequisite for this experiment is the vacuum state, because in the vacuum state there is no probability of other gases infecting the drug in the bottle. Put the experimental medicine into the bottle, extract the air inside through the vacuum machine, and then heat the bottle.

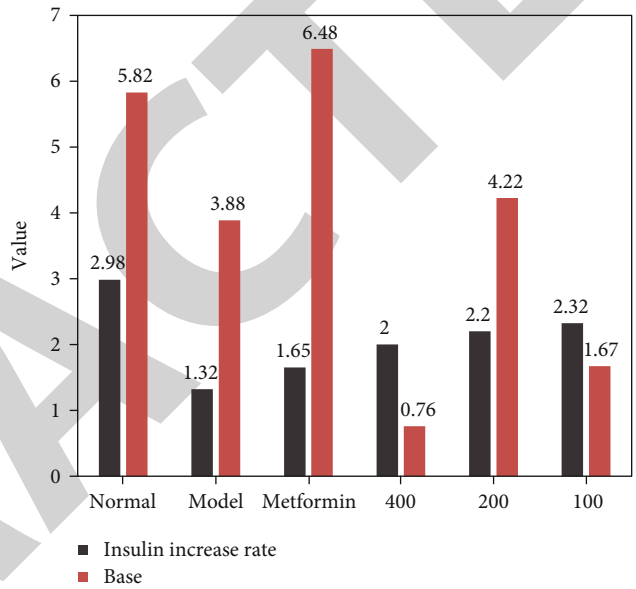

Figure 6: Effect of EGCG3″Me on glucose-stimulated insulin release in diabetic mice ($\bar{x} \pm s$, $n = 11$).

3.2. Pathogenesis and Treatment Status of t2dm. It has been confirmed that the pathogenesis of T2DM mainly includes pancreatic islet cell β-cell dysfunction and insulin resistance (IR) produced by peripheral tissues and cells. Insulin is the only hormone in the body that lowers blood sugar. It plays a decisive role in maintaining the body's blood glucose dynamic balance. It plays a role in maintaining a constant blood sugar in the peripheral target tissues (such as skeletal muscle, fat, and liver). Therefore, improving the function of pancreatic β-cells and inhibiting insulin resistance are

Table 2: Effects of EGCG3″Me on serum lipids in diabetic mouse models induced by STZ ($\bar{x} \pm s$, $n = 11$).

Group	Dose (mg/kg)	T-CHO (mmol/L)	TG (mmol/L)	LDL-C (mmol/L)	HDL-C (mmol/L)
Normal	—	2.50 ± 0.54	2.13 ± 0.68	0.23 ± 0.078	1.63 ± 0.24
Model	—	$4.95 \pm 0.83^{\#\#\#}$	$5.43 \pm 1.41^{\#\#\#}$	$0.50 \pm 0.11^{\#\#\#}$	$0.67 \pm 0.12^{\#\#}$
Metformin	400	$2.83 \pm 0.69^{***}$	$3.02 \pm 0.64^{**}$	$0.25 \pm 0.10^{***}$	$1.50 \pm 0.40^{***}$
EGCG3″Me high dose	400	$3.29 \pm 0.90^{**}$	$3.26 \pm 0.61^{**}$	$0.27 \pm 0.06^{***}$	$1.70 \pm 0.33^{***}$
EGCG3″Me medium dose	200	$3.39 \pm 1.34^{*}$	$3.35 \pm 0.91^{**}$	$0.30 \pm 0.075^{***}$	$1.86 \pm 0.29^{***}$
EGCG3″Me low dose	100	$3.54 \pm 1.06^{*}$	$3.82 \pm 0.82^{*}$	$0.26 \pm 0.11^{***}$	$1.32 \pm 0.47^{*}$

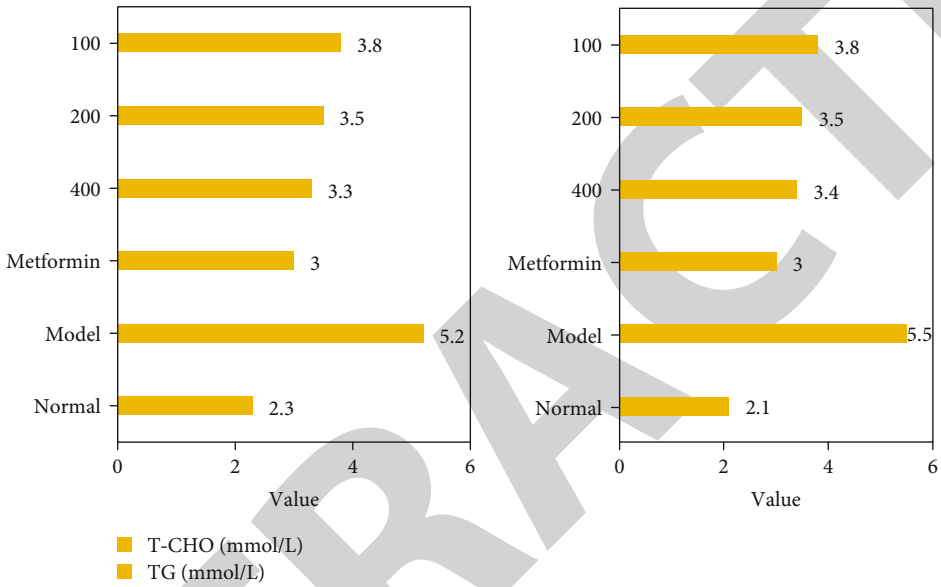

Figure 7: The effect of EGCG3″Me on serum T-CHO and serum TG levels in diabetic mice ($\bar{x} \pm s$, $n = 11$).

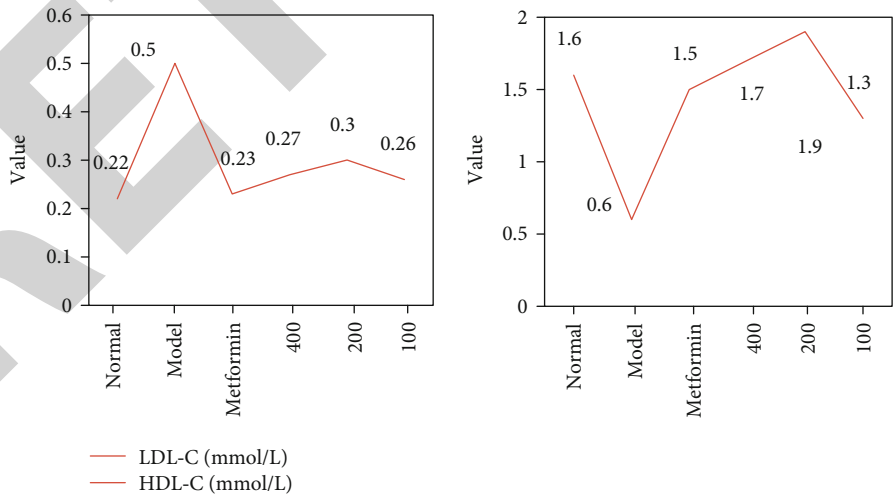

Figure 8: Comparison of the effects of EGCG3″Me on serum LDL-C and serum HDL-C levels in diabetic mice ($\bar{x} \pm s$, $n = 11$).

the key to the prevention and treatment of T2DM. T2DM is currently a clinical treatment drug, mainly western medicine, including various long-acting, medium-acting and short-acting insulin, anticarbohydrate absorption agents, and other injection drugs. Although these western medicines have definite curative effects, they have shorter effects and many side effects. Long-term use will reduce the curative effect and increase the economic burden. For this reason, it

is necessary to find a prevention and treatment method for T2DM with a wide range of sources, long-lasting effects, and small side effects.

3.3. Research Progress of EGCG3″Me in the Field of Prevention and Treatment of t2dm. Scientists have verified that transplanting stem cells can improve pancreatic β-cell function and inhibit insulin, thereby treating type 2 diabetes. It shows that EGCG3″Me can inhibit the insulin resistance of skeletal muscle cells. In addition, EGCG3″Me can also inhibit insulin-induced hepatocyte HepG2 apolipoprotein B (ApoB) secretion. Excessive liver ApoB is closely related to insulin resistance caused by lipid metabolism disorders.

3.4. Establishment of Diabetes Mouse Model

3.4.1. Preparation of Sodium Citrate Buffer Solution. The citric acid solution and sodium citrate solution are mixed in equal amounts, fine-tuned, and the pH value is measured with a pH test paper, so that the pH value is between 4.2 and 4.5. The configured buffer is filtered with a 0.22 μm microporous membrane, sealed, and stored at 4°C.

3.4.2. Model Building and Group Administration. Take 120 male mice from a certain province, and divide them into a blank group with 11 models and 109 models. After 12 hours of fasting, STZ was injected into the abdominal cavity of the model. STZ was dissolved in the abdominal cavity with 0.1 mmol/L sterile citric acid-sodium citrate buffer (150 mg/L).

Respectively, on the 7th, 14th, 21st, 28th, and 35th days of administration, blood was collected from the tail vein after 12 hours of fasting in advance, and fasting blood glucose was measured with a blood glucose meter.

3.5. Glucose Tolerance Test in Diabetic Mice and Glucose-Stimulated Insulin Release Test. After fasting for 12 hours, blood was collected from the capillary orbital venous plexus. The mice were given 20% glucose solution (2 g/kg body weight) by gavage. After 10 minutes, the mice had their eyes removed and blood was collected. The blood glucose level of 10 min and the serum insulin level of 0 min and 10 min were measured, respectively. G10 represents the blood glucose level when the glucose load is 10 min, and InS0 and InS10 are the blood glucose insulin levels at the time points of 0 and 10 min after the glucose load, respectively. The insulin increase rate of each group of mice is calculated [(Ins10-Ins0)/InS0].

4. Experimental Results

4.1. General State of Mice. The mice in the blank group are in good health and good spirits and have medium body shape, steady weight gain, shiny hair, free movement, and no significant changes in water intake, food intake, and defecation volume. The mice in the model group are in poor condition, lethargic, and lean; weight gain is slow; hair is dull; and water intake and food intake increased significantly. The performance of mice in each drug group improved to varying degrees.

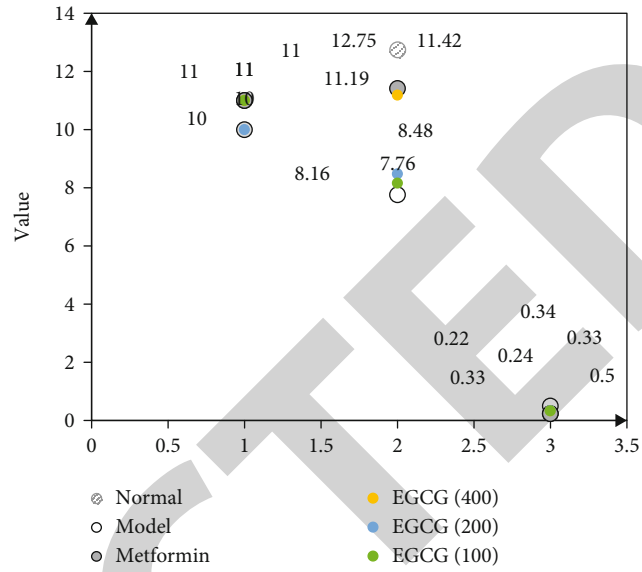

Figure 9: Effect of EGCG3″Me on liver glycogen and liver triglyceride content in diabetic mice ($\bar{x} \pm s$).

4.2. EGCG3″Me Impact Analysis

4.2.1. The Effect of EGCG3″Me on Fasting Blood Glucose in Diabetic Mice. The results of the test are shown in Figure 4. The fasting blood glucose level of mice in the fasting blood glucose group did not fluctuate significantly during the medication period and was at a normal level, and the fasting blood glucose level was always at a higher level compared with the blank group ($P < 0.001$). After 14 days of administration, the fasting blood glucose of the mice in the metformin group and EGCG3″Me high-, medium-, and low-dose groups began to decrease; the blood glucose level of the metformin treatment group was significantly lower than that of the model group ($P < 0.01$) and was lower than the model group ($P < 0.05$) .

4.2.2. The Effect of EGCG3″Me on Glucose Tolerance in Diabetic Mice. The results of the experiment are shown in Figure 5. After the mice in each group were given glucose, the blood glucose level increased to varying degrees, and the blood glucose value reached the maximum value at 30 minutes. The blood glucose levels of the mice in the blank group were basically restored to normal levels when they were given glucose for 60 minutes and 120 minutes. The range of blood glucose fluctuations in the metformin group and EGCG3″Me high-, medium-, and low-dose groups was relatively small, indicating that metformin and EGCG3″Me can alleviate the impaired glucose tolerance of diabetic mice.

4.2.3. The Effect of EGCG3″Me on Glucose-Stimulated Insulin Release in Diabetic Mice. As shown in Table 1 and Figure 6, after 12 hours of fasting, the 0 min serum insulin concentration of the model group was significantly lower than that of the blank group. After the same dose of glucose was stimulated for 10 minutes, while the blood glucose of each group increased, the increase in the insulin secretion

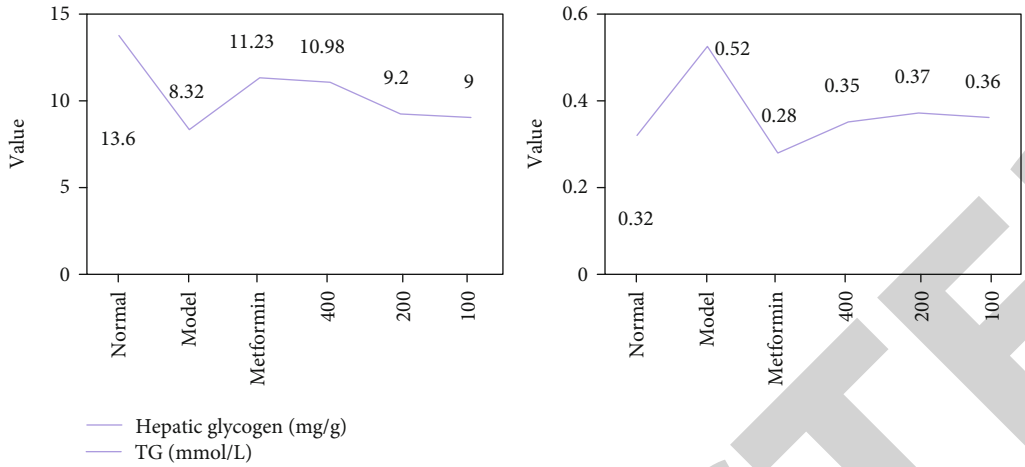

Figure 10: Comparison of the effects of EGCG3″Me on liver triglycerides and liver glycogen ($\bar{x} \pm s$).

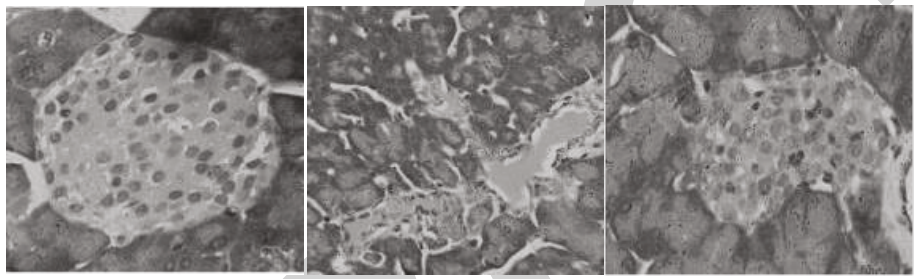

Figure 11: HE staining diagram of blank group, model group, and metformin group.

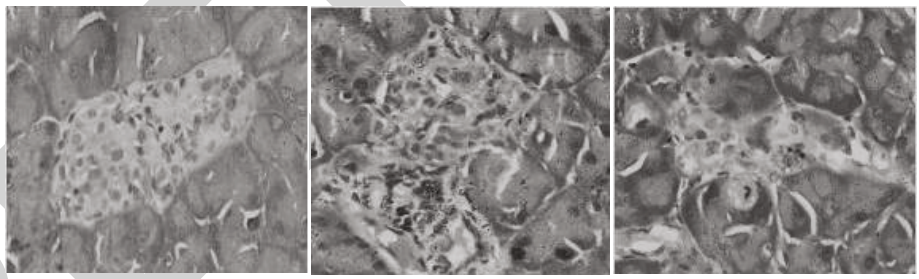

Figure 12: HE staining diagram of EGCG3″Me high-, medium-, and low-dose groups.

level also changed significantly. At 10 minutes in the model group, the EGCG3″Me level was significantly lower than that of the blank group ($P < 0.01$), and the percentage of insulin increase is significantly lower than that of the blank group.

4.2.4. Observe the Effect of EGCG3″Me on Serum Lipid Metabolism in Diabetic Mice. The test results are shown in Table 2 and Figures 7 and 8: the total cholesterol content of mice in the model group was significantly higher than that of the blank group; compared with the model group, the total cholesterol content of the metformin group was significantly lower than that of the model group ($P < 0.001$).

4.2.5. The Effect of EGCG3″Me on Liver Triglycerides and Liver Glycogen in Diabetic Mice. As shown in Figures 9 and 10, compared with the blank group, the liver glycogen content of the model group was significantly decreased ($P < 0.001$), while those of the high-dose group and EGCG3″Me group were significantly increased ($P < 0.001$).

4.3. HE Staining Results of Mouse Pancreas. The HE staining of mouse pancreas tissue in each group is shown in Figures 11 and 12. The pancreas of the normal group of mice have full acinar cells, less paging of acinar cells, more pancreatic islets, complete cell morphology, tightly arranged, approximately round or elliptical, rich intracellular cytoplasm, dark oval nucleus, and centered position. Acinar

paging increased in the medium-dose group of EGCG3″Me, and a few had blurred borders. In the low-dose EGCG3″Me group, there were many acinar paging, few pancreatic islet cells, irregular morphology, and blurry borders.

Glucose homeostasis depends to a large extent on the fine-regulated balance between insulin sensitivity and output in the pancreas, and insulin abnormalities require a corresponding increase in insulin output to maintain normal blood glucose levels. Influencing β-cell function and viability is related to metabolic abnormalities such as glucose toxicity, lipotoxicity, oxidative stress, and inflammation. Abnormal insulin metabolism in β-cells is due to impaired phosphorylation activation of insulin receptor substrate proteins, which leads to impaired glucose transduction and increases β-cell loss.

5. Conclusions

The drug streptozotocin, which triggers the diabetes model in this study, can damage pancreatic β-cells through its specific action on DNA, reduce the number of pancreatic β-cells, and significantly increase the degranulation of residual β-cells, resulting in decreased insulin synthesis and secretion.. In this study, through glucose-stimulated insulin release experiments and pancreatic HE staining, it was found that the pancreatic islet cells of the diabetic mice were significantly damaged, the number of acinar paging increased, and the number of cells in the pancreatic islets decreased. Compared with the model group, the number of acinar paging and the number of cells in the pancreatic islets increased in the mice after EGCG3″Me treatment, indicating that EGCG3″Me has the effect of protecting and repairing pancreatic islet cells.

Data Availability

No data were used to support this study.

Conflicts of Interest

The author(s) declare(s) that they have no conflicts of interest.

References

[1] J. Zhang, S. Tang, and D. Li, "On the molecular mechanism of Liuweidihuang Pills in the treatment of diabetes based on integrated pharmacology," *Complex systems and complexity Science*, vol. 15, no. 1, pp. 24–30, 2018.

[2] L. Qin and T. Wang, "Design and research of automobile anti-collision warning system based on monocular vision sensor with license plate cooperative target," *Multimedia Tools and Applications*, vol. 76, no. 13, pp. 14815–14828, 2017.

[3] Y. Abbasi, S. Moosavian, and A. B. Novinzadeh, "Vision-based formation control of aerial robots in the presence of sensor failure," *Journal of Mechanical Science & Technology*, vol. 31, no. 3, pp. 1413–1426, 2017.

[4] A. Masson, C. Haskamp, and I. Ahrns, "Airbus DS Vision Based Navigation solutions tested on LIRIS experiment data," *Journal of the British Interplanetary Society*, vol. 70, no. 2-3-4, pp. 152–159, 2017.

[5] K. Sakuma, W. Aoi, and A. Yamaguchi, "Molecular mechanism of sarcopenia and cachexia: recent research advances," *Pflügers Archiv-European Journal of Physiology*, vol. 469, no. 5-6, pp. 573–591, 2017.

[6] T. Bosona, G. Gebresenbet, and F. S. Bulitta, "Cellular and molecular mechanisms of secondary neuronal injury following traumatic brain injury – translational research in traumatic brain injury," *Livestock Science*, vol. 142, no. 1, pp. 138–146, 2016.

[7] M. K. Choi, O. K. Park, C. Choi et al., "Cephalopod-inspired miniaturized suction cups for smart medical skin," *Advanced Healthcare Materials*, vol. 5, no. 1, pp. 80–87, 2016.

[8] Y. X. He, Y. Zhu, and L. J. Yang, "Research progress of NDRG1 in molecular mechanism of tumor invasion and metastasis," *Zhonghua Bing LI Xue Za Zhi Chinese Journal of Pathology*, vol. 47, no. 1, pp. 75–78, 2018.

[9] X. Z. Liu, L. T. Zhang, and W. Q. Tong, "Research advances in molecular mechanisms of the invasion and metastasis of lung cancer," *Acta Academiae Medicinae Sinicae*, vol. 38, no. 1, pp. 108–112, 2016.

[10] P. Liczbiński and B. Bukowska, "Molecular mechanism of amygdalin action in vitro: review of the latest research," *Immunopharmacology and Immunotoxicology*, vol. 40, no. 3, pp. 212–218, 2018.

[11] S. Huang, N. Rao, and S. Xu, "Research progress on the cellular and molecular mechanisms of tooth eruption," *West China Journal of Stomatology*, vol. 34, no. 3, pp. 317–321, 2016.

[12] M. C. Pan, X. W. Zhou, and Y. Liu, "Research progress on the molecular mechanisms of toxicology of ethanol-aconitine induced arrhythmia," *Fa Yi Xue Za Zhi*, vol. 36, no. 1, pp. 115–119, 2020.

[13] Y. Kim, G. Obinata, and B. Kawk, "Vision-based fluid-type tactile sensor for measurements on biological tissues," *Medical & Biological Engineering*, vol. 56, no. 3, pp. 1–9, 2017.

[14] H. Li and C. Zhong, "A machine vision based autonomous navigation system for lunar rover: the model and key technique," *Sensor Review*, vol. 36, no. 4, pp. 377–385, 2016.

[15] J. Fan, F. Jing, and Y. Lei, "A precise initial weld point guiding method of micro-gap weld based on structured light vision sensor," *IEEE Sensors Journal*, vol. 19, no. 1, pp. 322–331, 2019.

[16] P. Xiao and L. Zhen, "High-accuracy calibration of line-structured light vision sensor by correction of image deviation," *Optics Express*, vol. 27, no. 4, pp. 4364–4385, 2019.

[17] C.-H. Yu-Yang, "research progress on molecular mechanism of Dendrobium officinale and its active components to metabolic syndrome," *China journal of Chinese materia medica*, vol. 44, no. 23, pp. 5102–5108, 2019.

[18] S. Chen, B. Gavish, and S. Zhang, "Monitoring of erythrocyte aggregate morphology under flow by computerized image analysis," *Biorheology*, vol. 32, no. 4, pp. 487–496, 1995.

[19] J. Weickert, S. Grewenig, C. Schroers, and A. Bruhn, "Cyclic schemes for PDE-based image analysis," *International Journal of Computer Vision*, vol. 118, no. 3, pp. 275–299, 2016.

[20] D. J. Jose, "Instrumental techniques to quantify textural change in carpet part I: image analysis," *Textile Research Journal*, vol. 56, no. 10, pp. 591–597, 2016.

[21] N. Mizoue, "CROCO: semi-automatic image analysis system for crown condition assessment in Forest Health Monitoring," *Journal of Forest Planning*, vol. 8, no. 3, pp. 17–24, 2017.